Letter

Thermalization slowing down in multidimensional Josephson junction networks

Gabriel M. Lando and Sergej Flach
Center for Theoretical Physics of Complex Systems, Institute for Basic Science (IBS), Daejeon 34126, South Korea

(Received 4 July 2023; accepted 30 November 2023; published 28 December 2023)

We characterize thermalization slowing down of Josephson junction networks in one, two, and three spatial dimensions for systems with hundreds of sites by computing their entire Lyapunov spectra. The ratio of Josephson coupling E_J to energy density h controls two different universality classes of thermalization slowing down, namely, the weak-coupling regime, $E_J/h \to 0$, and the strong-coupling regime, $E_J/h \to \infty$. We analyze the Lyapunov spectrum by measuring the largest Lyapunov exponent and by fitting the rescaled spectrum with a general ansatz. We then extract two scales: the Lyapunov time (inverse of the largest exponent) and the exponent for the decay of the rescaled spectrum. The two universality classes, which exist irrespective of network dimension, are characterized by different ways the extracted scales diverge. The universality class corresponding to the weak-coupling regime allows for the coexistence of chaos with a large number of near-conserved quantities and is shown to be characterized by universal critical exponents, in contrast with the strong-coupling regime. We expect our findings, which we explain using perturbation theory arguments, to be a general feature of diverse Hamiltonian systems.

DOI: 10.1103/PhysRevE.108.L062301

Thermalization has been a central concept in theoretical physics since the birth of statistical mechanics. It allows for an explanation as to how time-dependent microscopic dynamics gives birth to macroscopic equilibrium, and is deeply rooted in the classical concepts of chaos and ergodicity [1–6]. Here, the assumption that all arbitrary initial conditions lead to the same long-time average when dynamics is sufficiently ergodic—and, therefore, that time averages and ensemble averages are interchangeable—is fundamental. It is then natural to wonder what happens when systems that obey this *ergodic hypothesis* approach a limit in which it ceases to be valid. In the context of many-body Hamiltonian dynamics, which lies beyond the applicability horizons of Kolmogorov-Arnol'd-Moser (KAM) theory [7–10], this matter can be envisaged as the study of how chaotic many-body systems approach integrability.

Since thermalization is reflected in the behavior of long-time averages, investigations so far have privileged its diagnose by computing classical expectation values [11–13]. This introduces unnecessary moving parts, e.g., choices of coordinates and classical observables, with "good" choices often obscured [14]. As a consequence, recent work has instead focused on Lyapunov spectra (LS). Contrary to observables, LS are coordinate-independent and invariant under a wide range of transformations [15], providing a complete measure of chaos and its characteristic timescales for any classical system [16–18]. In a recent paper they were employed to show that a specific class of discrete one-dimensional unitary maps, similar to nonlinear quantum random talks, thermalize *via* two different pathways depending on whether the target integrable limit decouples interactions in real or reciprocal space [18]. However, due to substantial computational challenges, little to nothing is currently known about how many-body Hamiltonian systems cease to thermalize, and whether their thermalization slowing-down processes fit the universality classes discovered in Ref. [18].

In this Letter, we characterize the thermalization slowing down of classical Hamiltonian systems with hundreds of degrees of freedom, addressing the issue mentioned above and showing these universality classes are a general property of Hamiltonian lattices in any dimension. Our analysis is based on a direct computation of the full LS, for which we introduce an ansatz capable of fitting the spectra in any perturbation regime. The models chosen are one-, two- and three-dimensional (1d, 2d, and 3d) Josephson junction networks, which have been extensively studied in 1d as a probe to the richness of one-dimensional physics [19–24], and in 2d as an exact analog of the XY chain, offering the possibility of simulating a multitude of statistical phenomena in chips [25,26]. Our calculations show that the models thermalize according to two different universality classes near their integrable limits depending on the network type—either short-ranged or long-ranged (essentially all-to-all), spanned by the weak nonintegrable perturbation over the set of actions (which are integrals of motion at the very limit [12,27]). In the long-range network (LRN) regime the LS is always well approximated by an analytical function that depends only on the maximal Lyapunov exponent (mLE). The short-range network (SRN) regime is drastically different, with LEs decreasing exponentially according to a second diverging scale, the *spectral decay rate*, rendering thermalization extremely slow when compared with the Lyapunov time (the inverse of the mLE).

Both the Lyapunov time and the spectral decay rate are shown to be remarkably universal in the SRN class through the extraction of scaling laws and their critical exponents. The LRN class is not characterized by additional universal scaling laws, a phenomenon we explain by invoking classical perturbation theory. In the SRN class, near-zero and large LEs coexist, such that regular submanifolds are gradually reconstructed within a sea of strong chaos as the integrable limit is

approached. Such coexistence is absent in the LRN class, in which chaos vanishes almost evenly and tori are rebuilt nearly all at once. This suggests that the transition to integrability in the SRN and LRN classes, if interpreted as a phase transition, can be of more than one type (e.g., first or second order).

Our findings can be used to interpret equipartition, thermalization and ergodicity both in experimental and theoretical investigations, and we expect them to be useful in the analysis of any system displaying long- and/or short-range interactions, and many-body localization.

We now introduce the systems employed throughout the rest of this Letter. Denoting momentum and position by $\mathbf{p}$ and $\mathbf{q}$, the Hamiltonians for all networks considered here have the general form

$$H(\mathbf{p},\mathbf{q}) = \frac{|\mathbf{p}|^2}{2} + E_J \sum_{\langle\sigma_1,\sigma_2\rangle} [1-\cos(q_{\sigma_1}-q_{\sigma_2})], \quad (1)$$

where E_J is the Josephson coupling between two neighboring superconducting islands, and σ_1, σ_2 are multi-indices counting nearest neighbors. Associated with each component of position there is a momentum p entering the kinetic term, such that $p^2/2$ is interpreted as the island's Coulomb charging energy, and the rotor angle q as the phase of the superconducting order parameter. For the 1d network we assume periodic boundary conditions, while for the 2d and 3d cases—which we take as a square and a cube lattices with edge N—we leave them open. We refer to different dimensionalities implicitly by writing the total number of sites as N, N^2, and N^3 for $d = 1, 2$, and 3, e.g., the circular ring with 120 sites and the $5 \times 5 \times 5$ cube will be referred to as $N = 120$ and $N = 5^3$.

The Josephson junction networks (1) conserve both total momentum and energy. The former can always be set to zero due to the Galilean invariance of macroscopic systems, or periodic boundary conditions. The relevant parameters are then the energy density, $h = H/N$ and E_J. Due to the boundedness of the potential-energy term in (1), $h \to 0$ can only be achieved for fixed E_J by constraining $q_{\sigma_1} - q_{\sigma_2}$ and $\mathbf{p}$ to be small. The cosine can then be expanded as $\cos x \approx 1 - x^2/2$ and, for small energies, the networks become integrable sets of coupled harmonic oscillators. The same effect can be realized as $E_J \to \infty$ while keeping h fixed, such that $E_J/h \gg 1$ takes care of both possibilities and furnishes what we refer to as the LRN regime, in which sites remain strongly connected. The opposite case $E_J/h \ll 1$ produces the SRN regime, in which the sites become weakly coupled sets of rotors or nearly disconnected superconducting islands.

We enter the SRN and LRN regimes by varying different parameters, namely $(E_J \to 0, h = 1)$ for the first and $(E_J = 1, h \to 0)$ for the latter, with the data continuously glued together using the simple rescaling transformations described in Ref. [27]. This is only possible because the Hamiltonian (1) has effectively a single parameter, namely E_J/h, in terms of which we present our results [28].

Since we are interested in the vicinity of integrable limits, the dynamics is weakly chaotic and the time necessary to resolve LEs is very long. This reliance on long times, together with the fact that we would like to preserve conserved quantities as much as possible in order to avoid creating "fake" chaos due to numerical instabilities, lead to the need of employing symplectic integrators [30–33]. Here, we employ the second-order optimized method of Ref. [31] for solving the equations of motion for the monodromy matrix $\mathcal{M}$, i.e., the Jacobian of the Hamiltonian flow, Φ:

$$\frac{d\mathcal{M}(\mathbf{z};t)}{dt} = \mathcal{J}\,\mathrm{Hess}\,H(\mathbf{z}')\Big|_{\mathbf{z}'=\Phi(\mathbf{z};t)}\,\mathcal{M}(\mathbf{z};t). \quad (2)$$

In the above, $\mathbf{z} = (\mathbf{p},\mathbf{q})$ denotes a $2N$-dimensional phase-space variable composed of N momentum-position pairs, H is the system's Hamiltonian, and $\mathcal{J}$ is the symplectic matrix [7,8]. The initial point $\mathbf{z}$ is evolved to $\mathbf{z}' = \Phi(\mathbf{z};t)$ by the Hamiltonian flow, which is computed in parallel. We then extract the LS from $\mathcal{M}$ by employing the well-known QR-decomposition algorithm of Ref. [34]. This method, which is both accurate and efficient for continuous systems [35,36], works especially well if small times steps dt are used. This is what led us to choose a low-order algorithm with small dt instead of the standard prescription, i.e., a high-order one with large dt [36–38]. Here, we fix the step size as $dt = 0.2$ for all models considered, with final propagation times of $t_f = 2 \times 10^6$ for 1d and 2d systems, and 10^6 for the 3d case. This results in a relative energy and total momentum drifts no larger than 10^{-3} and 10^{-12}, respectively, with small variations depending on the number of sites and dimensionality [27].

Since the computed LS will be very different depending on the system's parameters, we rescale them in order to facilitate comparisons. The rescaling transformation for each LE is simply $\overline{\Lambda}_i = \Lambda_i/\Lambda_1$, where $\Lambda_1 > \Lambda_2 > \ldots > \Lambda_{N-1} = \Lambda_N = 0$ are the original LEs, the last two being equal to zero due to total momentum and energy conservation. Since we work with systems with several different sizes, we also define a rescaled x axis, namely, $\rho = \{i/N\}_i$. This results in plots for the rescaled spectra that vary between 0 and 1 both in the y as in the x axes, as can be seen in the set of LS displayed in Fig. 1. The E_J/h values and the number of sites for each row can be seen as insets in the panels on the right. We also keep track of the mLEs, which are shown for several system sizes and dimensionalities in Fig. 2.

To provide a more quantitative distinction between SRN and LRN regimes, we employ a modification of an ansatz suggested in Ref. [17] in which the rescaled LS away from integrable limits is approximated as $1 - \rho^\alpha$. Our modification arises from noticing that LS in the SRN regime appear to decay exponentially as a function of ρ, such that the new ansatz

$$\overline{\Lambda(\rho;\alpha,\beta)} = (1-\rho^\alpha)\,e^{-\beta\rho} \quad (3)$$

should also take care of the SRN regime. In Fig. 1 one can see that least-squares fits, obtained from a Marquadt algorithm with input (3), provide excellent approximations in both the SRN and LRN regimes [39]. The coefficients β, therefore, provide a measure of the spectral decay rates, which are displayed in the SRN regime as insets in Fig. 1. The critical exponent ν is then obtained as the angular coefficient of a

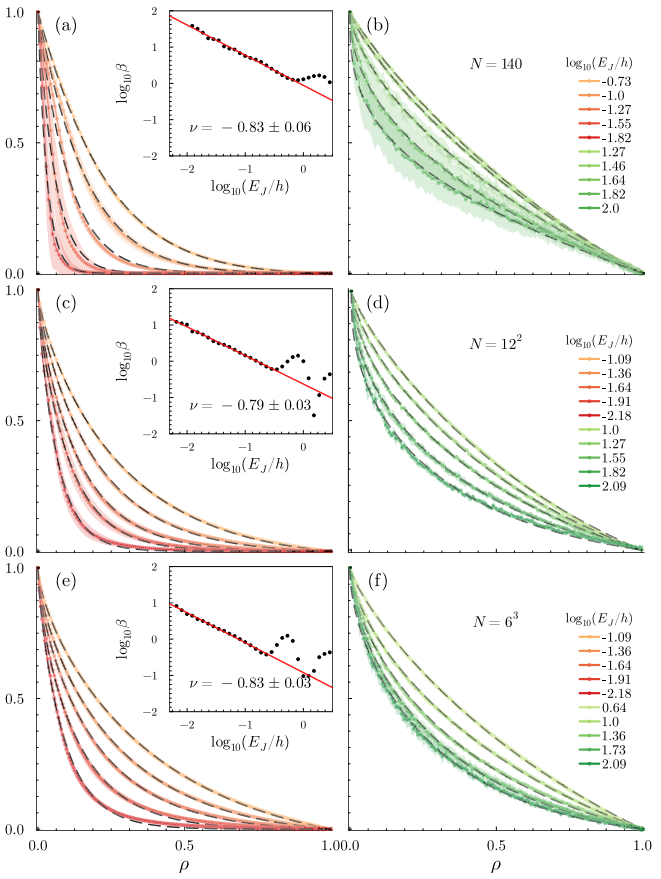

FIG. 1. Selected sets of rescaled Lyapunov spectra $\bar{\Lambda}(\rho)$ in the short-range regime (red and orange tones) for the (a) 1d, (c) 2d, and (e) 3d networks, together with the fits obtained from the ansatz (3) (black dashed curves). The variable ρ is a normalized counting index. The insets show the β coefficients in (3), which measure the speed of exponential decay, together with a power-law fit with exponent ν. (b), (d), (f) Same, but in the long-range regime in which no exponential decay is visible and the Lyapunov exponents do not bend towards zero. For all plots, error bars are computed from runs with different initial conditions and shown as ribbons [27], and the values of E_J/h and system sizes and dimensionalities are shown in the panels on the right.

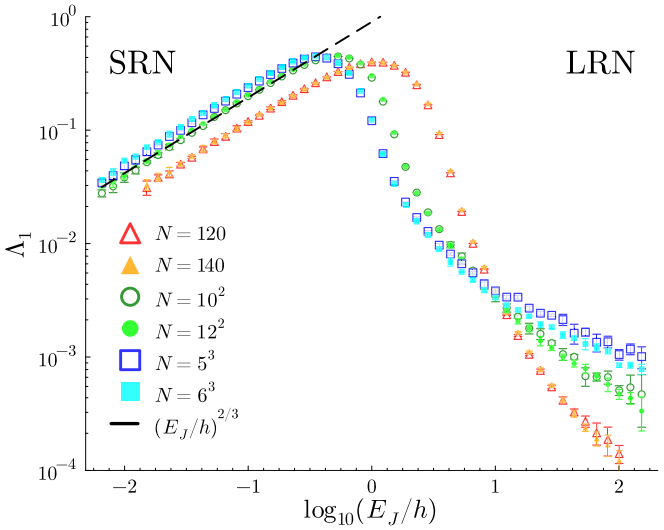

FIG. 2. Maximal Lyapunov exponent versus $\log_{10} E_J/h$ for all networks. Solid markers denote the same configuration as their open counterparts, but with a larger number of sites. The solid black line shows a power-law with critical exponent $2/3$, predicted analytically in Ref. [29].

linear fit to $\log_{10}\beta$ vs $\log_{10}(E_J/h)$ and shown to be universal and independent of boundary conditions, number of sites and even dimensionality, as can be seen in more detail in Fig. 3. In the latter we also display the robustness of our results by comparing between fit parameters obtained from different system sizes. We also note that (3) will be useful in an analytical approach to thermalization slowing down and provides, among other things, an analytical expression for the Kolmogorov-Sinai entropy (see, e.g., Ref. [40]).

As can be easily seen in the left panels of Fig. 1, and particularly for the 1d network, the SRN regime is characterized by a LS that is strongly dominated by a small subset of LEs, the majority of the others bending towards zero. Although the rate with which the LEs bend down decreases with increasing dimensionality, a comparison with the panels on the right renders the distinction between LRN and SRN unmistakable, since LEs in the latter remain steadily above zero—with the exception of those associated with the two conserved quantities. This dramatic contrast between SRN and LRN regimes justifies referring to thermalization slowing down as arising in two distinct universality classes (UCs), depending on which integrable regime is neared. The fundamental distinction between the LRN and SRN UCs is, as previously mentioned, the network range spanned by the nonintegrable perturbation among the actions of the integrable limit system [12,27]. As a result, in the LRN class the sites remain strongly coupled as the integrable limit is approached, while decoupling in the SRN class.

It is enlightening to recast the previously described UCs in the language of classical perturbation theory, which cannot be properly applied for the maps studied in Ref. [18]. In their integrable limits, both UCs allow for a description in terms of action-angle coordinates, in which the N actions provide a full set of conserved quantities in involution [7,8]. In the SRN-UC the actions of the unperturbed integrable system are given by the kinetic energy of each uncoupled site, while in the LRN-UC they are the normal modes. Therefore, the actions are spatially extended in the latter, and localized in the former. Once the systems are perturbed, chaos enters the LRN-UC in the form of nonlinearly coupled normal modes interacting with each other in an all-to-all fashion, while in the SRN-UC it comes in the form of sparse isolated resonance pockets between weakly interacting nearest-neighbor rotors [41,42]. Those pockets are the source of strongest chaos and the main responsible for the magnitude of the mLE in the SRN regime.

Due to the extended nature of perturbed actions in the LRN-UC, any normal mode will be involved in at least one chaotic resonant interaction [43], with probability exponentially close to one [27]. Therefore, in this black and white picture in which a mode is either resonant or not, all LEs should be of the same order of magnitude, confirming that the rescaled LS should approach a stationary curve. At variance,

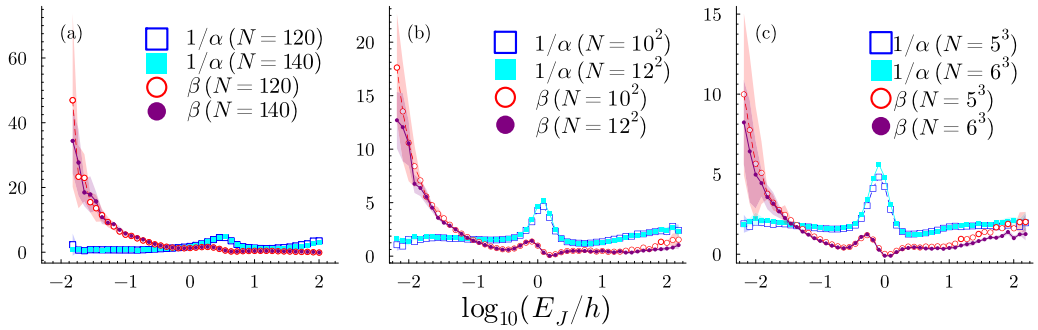

FIG. 3. Fit coefficients for the ansatz (3) for two sizes of the (a) 1d, (b) 2d, and (c) 3d networks. A log-log plot which clearly displays the power-law behavior of the β coefficients can be seen in the insets of Fig. 1. Note that we plot $1/\alpha$ instead of α for ease of visualization. Error bars are displayed as ribbons.

for the SRN-UC a rotor will be involved in a resonance with at least one of its nearest neighbors with a small probability, namely $2d\,E_J/h$ [27]. Such sparse resonant pockets have an average distance of $\approx(h/E_J)^{1/d}/d^{1/d}$. Therefore the mLE should show a similar dependence on E_J/h for any dimension, and most of the other LEs should become negligibly small compared with the mLE, confirming the observed exponential decay of the LS.

The above development helps us understand several facets of Figs. 1 and 2. First, due to the sites interacting only with their nearest neighbors, it explains why the mLEs in Fig. 2 scale according to the same critical exponent in the SRN-UC, predicted analytically to be $2/3$ for the 1d chain [29] (see also Ref. [44]) and shown here, perhaps surprisingly, to be the same for all dimensionalities.[1] This has to be contrasted with the LRN-UC, in which all normal modes interact with each other and increasing the system's dimensionality strongly impacts the dynamics, since the number of almost-resonant normal modes increases: 1 or 2 for $d=1$ (depending on the boundary conditions), and $\approx N^{d-1}$ for higher dimensions. This explains the smaller slopes of the LRN spectra in Fig. 2 as a function of increasing dimensionality—larger systems are more chaotic and, therefore, the speed at which they stop thermalizing is slower. Interestingly, this is also reflected in our computational simulations, in the sense that to achieve convergence in the LRN regime we need considerably shorter times when dealing with 2d and 3d systems when compared with 1d ones.

The earlier localization argument also applies to the observed universality in the second critical exponent that characterizes the SRN-UC, denoted as ν in the insets of Fig. 1: Since the speed at which exponentially decaying LS curves bend towards zero can only depend on nearest neighbors, the exponent ν should not depend on dimensionality at all. This is in strong contrast with the LRN-UC, in which the plots in Fig. 3 point to the possible existence of an asymptote that, at present, lies beyond our computational resolving power, but that has been already observed in 1d unitary circuits maps [18], and indications of which were reported for a short chain of interacting classical spins [16].

Although both SRN and LRN UCs reflect the fact that the systems stop thermalizing when an integrable limit is reached, the simultaneous presence of large and near-zero LEs in the SRN class is associated with the coexistence of near-conserved quantities and strong chaos—a characteristic that is completely absent in the LRN class. In the language of KAM theory, one can interpret the SRN road to integrability as the gradual formation of regular low-dimensional submanifolds within chaotic regions in phase space, which continuously become N-dimensional tori when the limit is reached. Here, the universality of critical exponents also shows that the speed at which regularity is reconstructed appears remarkably constant. For the LRN pathway, on the other hand, tori are rebuilt as the whole dynamics approaches regularity. If one interprets chaos and integrability as *dynamical phases* [45], the mechanisms for thermalization slowing down in the SRN and LRN classes are associated with different types of phase transitions.

An interesting future research direction concerns adding disorder. This would allow for an interpolation between different universality classes, since Anderson localization can force the normal modes to localize. An even more intriguing question concerns the corresponding quantum many-body case. We have good reasons to expect that quantizing a classical SRN system will lead to quantum many-body localization, which implicates in the complete destruction of thermalization at a finite distance from the integrable limit. On the other hand, the quantization of a LRN system will probably not destroy thermalization and keep the system in range of the eigenstate thermalization hypothesis.

G.M.L. acknowledges the financial support from the Institute for Basic Science (IBS) in the Republic of Korea through the Project No. IBS-R024-D1. We thank Marco Baldovin, Barbara Dietz, Emanuelle Dalla Torre, Yagmur Kati, Dario Rosa, Steven Tomsovic, Angelo Vulpiani, Weihua Zhang, and Tilen Čadež for fruitful discussions, and Robert McLachlan for pointing out the advantages described in Ref. [46].

[1] We note that, while Ref. [29] enters the SRN regime by varying the energy density, we do so by varying the Josephson coupling. The two strategies are not equivalent but can be bijectively mapped, as shown in our Supplemental Material [27]. Indeed, the scaling found by [29] in the SRN regime is $h^{-1/6}$, which using Eq. 1 of the Supplemental Material can be easily shown to result in a $h^{-2/3}$ scaling in our case.

[1] J. W. Gibbs, *Elementary Principles in Statistical Mechanics* (C. Scribner's Sons, Chicago, 1902).

[2] L. Boltzmann, *Lectures on Gas Theory* (University of California Press, 2022).

[3] A. Y. Khinchin, *Mathematical Foundations of Statistical Mechanics* (Courier Corporation, 1949).

[4] E. Fermi, P. Pasta, S. Ulam, and M. Tsingou, Studies of the Nonlinear Problems, Tech. Rep. [Los Alamos National Lab. (LANL), Los Alamos, NM (United States), 1955], https://doi.org/10.2172/4376203.

[5] L. D. Landau and E. M. Lifshitz, *Statistical Physics* (Elsevier, 2013), Vol. 5.

[6] G. Gallavotti, *Statistical Mechanics: A Short Treatise* (Springer Science & Business Media, 1999).

[7] V. I. Arnol'd, *Mathematical Methods of Classical Mechanics* (Springer Science & Business Media, 2013), Vol. 60.

[8] A. M. O. De Almeida, *Hamiltonian Systems: Chaos and Quantization* (Cambridge University Press, 1988).

[9] J. Pöschel, A lecture on the classical KAM theorem, Proc. Symp. Pure Math. **69**, 707 (2000).

[10] C. E. Wayne, The KAM theory of systems with short range interactions, I, Commun. Math. Phys. **96**, 311 (1984).

[11] T. Mithun, C. Danieli, Y. Kati, and S. Flach, Dynamical glass and ergodization times in classical Josephson junction chains, Phys. Rev. Lett. **122**, 054102 (2019).

[12] T. Mithun, C. Danieli, M. V. Fistul, B. L. Altshuler, and S. Flach, Fragile many-body ergodicity from action diffusion, Phys. Rev. E **104**, 014218 (2021).

[13] M. Iñarrea, R. González-Férez, J. P. Salas, and P. Schmelcher, Chaos and thermalization in a classical chain of dipoles, Phys. Rev. E **106**, 014213 (2022).

[14] M. Baldovin, A. Vulpiani, and G. Gradenigo, Statistical mechanics of an integrable system, J. Stat. Phys. **183**, 41 (2021).

[15] R. Eichhorn, S. J. Linz, and P. Hänggi, Transformation invariance of Lyapunov exponents, Chaos, Solitons Fractals **12**, 1377 (2001).

[16] V. Constantoudis and N. Theodorakopoulos, Nonlinear dynamics of classical Heisenberg chains, Phys. Rev. E **55**, 7612 (1997).

[17] S. Iubini and A. Politi, Chaos and localization in the discrete nonlinear Schrödinger equation, Chaos, Solitons Fractals **147**, 110954 (2021).

[18] M. Malishava and S. Flach, Lyapunov spectrum scaling for classical many-body dynamics close to integrability, Phys. Rev. Lett. **128**, 134102 (2022).

[19] L. J. Geerligs, M. Peters, L. E. M. De Groot, A. Verbruggen, and J. E. Mooij, Charging effects and quantum coherence in regular Josephson junction arrays, Phys. Rev. Lett. **63**, 326 (1989).

[20] E. Chow, P. Delsing, and D. B. Haviland, Length-scale dependence of the superconductor-to-insulator quantum phase transition in one dimension, Phys. Rev. Lett. **81**, 204 (1998).

[21] I. M. Pop, I. Protopopov, F. Lecocq, Z. Peng, B. Pannetier, O. Buisson, and W. Guichard, Measurement of the effect of quantum phase slips in a Josephson junction chain, Nat. Phys. **6**, 589 (2010).

[22] M. Mulansky, K. Ahnert, A. Pikovsky, and D. Shepelyansky, Strong and weak chaos in weakly nonintegrable many-body Hamiltonian systems, J. Stat. Phys. **145**, 1256 (2011).

[23] M. Pino, L. B. Ioffe, and B. L. Altshuler, Nonergodic metallic and insulating phases of Josephson junction chains, Proc. Natl. Acad. Sci. USA **113**, 536 (2016).

[24] K. Cedergren, R. Ackroyd, S. Kafanov, N. Vogt, A. Shnirman, and T. Duty, Insulating Josephson junction chains as pinned Luttinger liquids, Phys. Rev. Lett. **119**, 167701 (2017).

[25] R. Newrock, C. Lobb, U. Geigenmüller, and M. Octavio, The two-dimensional physics of Josephson junction arrays, Solid State Phys. **54**, 263 (2000).

[26] P. Martinoli and C. Leemann, Two dimensional Josephson junction arrays, J. Low Temp. Phys. **118**, 699 (2000).

[27] See Supplemental Material at http://link.aps.org/supplemental/10.1103/PhysRevE.108.L062301 for a comprehensive account of numerical and analytical details, including the sampling of initial points, convergence of results and error estimation, which includes Refs. [30–39,46–49].

[28] Y. Sadia, E. G. Dalla Torre, and A. Rajak, From prethermalization to chaos in periodically driven coupled rotors, Phys. Rev. B **105**, 184302 (2022).

[29] L. Casetti, C. Clementi, and M. Pettini, Riemannian theory of Hamiltonian chaos and Lyapunov exponents, Phys. Rev. E **54**, 5969 (1996).

[30] H. Yoshida, Construction of higher-order symplectic integrators, Phys. Lett. A **150**, 262 (1990).

[31] R. I. McLachlan and P. Atela, The accuracy of symplectic integrators, Nonlinearity **5**, 541 (1992).

[32] G. Benettin and A. Giorgilli, On the Hamiltonian interpolation of near-to-the identity symplectic mappings with application to symplectic integration algorithms, J. Stat. Phys. **74**, 1117 (1994).

[33] E. Hairer and C. Lubich, The life-span of backward error analysis for numerical integrators, Numer. Math. **76**, 441 (1997).

[34] G. Benettin, L. Galgani, A. Giorgilli, and J.-M. Strelcyn, Lyapunov characteristic exponents for smooth dynamical systems and for Hamiltonian systems; a method for computing all of them. Part 1: Theory, Meccanica **15**, 9 (1980).

[35] K. Geist, U. Parlitz, and W. Lauterborn, Comparison of different methods for computing Lyapunov exponents, Prog. Theor. Phys. **83**, 875 (1990).

[36] F. Mogavero, N. H. Hoang, and J. Laskar, Timescales of chaos in the inner solar system: Lyapunov spectrum and quasi-integrals of motion, Phys. Rev. X **13**, 021018 (2023).

[37] G. Wanner and E. Hairer, *Solving Ordinary Differential Equations II*, Springer Series in Computational Mathematics (Springer, Berlin, Heidelberg, New York, 1996), Vol. 375.

[38] J. Laskar and P. Robutel, High order symplectic integrators for perturbed Hamiltonian systems, Celest. Mech. Dyn. Astron. **80**, 39 (2001).

[39] LsqFit.jl: Least–Squares fitting in Julia, https://github.com/JuliaNLSolvers/LsqFit.jl (2019).

[40] A. Lakshminarayan and S. Tomsovic, Kolmogorov-sinai entropy of many-body Hamiltonian systems, Phys. Rev. E **84**, 016218 (2011).

[41] R. Livi, M. Pettini, S. Ruffo, and A. Vulpiani, Chaotic behavior in nonlinear Hamiltonian systems and equilibrium statistical mechanics, J. Stat. Phys. **48**, 539 (1987).

[42] R. Livi, A. Politi, S. Ruffo, and A. Vulpiani, Liapunov exponents in high-dimensional symplectic dynamics, J. Stat. Phys. **46**, 147 (1987).

[43] B. V. Chirikov, A universal instability of many-dimensional oscillator systems, Phys. Rep. **52**, 263 (1979).

[44] G. Parisi and A. Vulpiani, Scaling law for the maximum Lyapunov characteristic exponent of infinite product of random matrices, J. Phys. A: Math. Gen. **19**, L425 (1986).

[45] P. Butera and G. Caravati, Phase transitions and Lyapunov characteristic exponents, Phys. Rev. A **36**, 962 (1987).

[46] R. I. McLachlan and G. Quispel, What kinds of dynamics are there? Lie pseudogroups, dynamical systems and geometric integration, Nonlinearity **14**, 1689 (2001).

[47] K. J. Palmer, Exponential dichotomies, the shadowing lemma and transversal homoclinic points, in *Dynamics Reported*, edited by U. Kirchgraber and H. O. Walther (Vieweg+Teubner Verlag, Wiesbaden, 1988), Vol. 1, pp. 265–306.

[48] S. Choi and J. Vaníček, High-order geometric integrators for representation-free Ehrenfest dynamics, J. Chem. Phys. **155**, 124104 (2021).

[49] H. Kinoshita, H. Yoshida, and H. Nakai, Symplectic integrators and their application to dynamical astronomy, Celest. Mech. Dyn. Astron. **50**, 59 (1991).